# Nanoscale

Accepted Manuscript


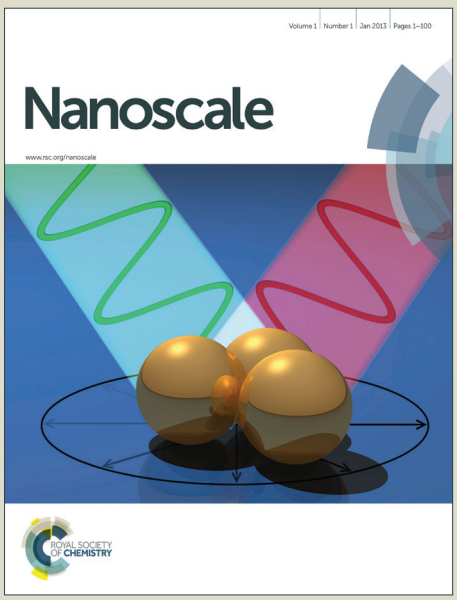





ROYAL SOCIETY OF CHEMISTRY

www.rsc.org/nanoscale

# Coarse-grained Modeling of Vesicle Responses to Active Rotational Nanoparticles

Liuyang Zhang and Xianqiao Wang*

College of Engineering and NanoSEC, University of Georgia, Athens, GA 30602, USA

## Abstract

In recent years, magnetically-driven-rotating superparamagnetic nanoparticles have been emerging as a valuable component to design targeted drug delivery carriers and cellular killers via membranes' physical rupture. The lack of an in-depth understanding of how to control the interaction of rotational nanoparticles (RNPs) with vesicles has hindered progress in the development of its relevant biomedical applications. Here we perform dissipative particle dynamics simulations to analyze the rotation frequencies, size, and coating patterns of the RNPs as they interact with the vesicle so as to provide novel designs of drug delivery applications. Results have revealed that the RNPs are capable to trigger local disturbance around the vesicle and therefore promote the vesicle translocation toward the RNPs. By investigating the translocation time and driving forces required for RNPs to enter inside of the vesicle under various rotation frequencies as well as the interaction energy between coated RNPs and the vesicle, we have tuned the coating pattern of the ligands on the surface of RNPs to open a specified channel in the vesicle for promoting the drug delivery. Our findings can provide useful guidelines for the molecular design of patterned RNPs for controllable bio/inorganic interfaces and help establish qualitative rules for the organization and optimization of ligands on the surface of desired drug delivery carriers.

**Keywords: dissipative particle dynamics, rotational nanoparticles, cellular uptake, cell membrane**



* Corresponding authors, Tel: 706-5426251; Email: xqwang@uga.edu

## Introduction

Recent years have witnessed the explosive growth of interest in nanoparticles (NPs) with a wealth of biomedical applications since they are widely used as carriers to translocate drug molecules and useful materials into cell interiors.[1] A number of simulation suggested that the membrane translocation of anisotropic NPs is often accompanied by spontaneous and continuous rotation of the NPs. Take the spontaneous rotation for example, the ligand coated NPs with anisotropic patterns rotated to preferred orientation while penetrating through the membrane.[2] Similar behavior was observed for the translocation of graphene sheets across the membrane.[3] In the endocytosis process of anisotropic NPs, the anisotropic NPs generally undergo a transient rotation during the wrapping process to minimize the free energy.[4, 5] Different from the limited effect of spontaneous rotation of anisotropic NPs, the promoting effect of continuous NP rotation is ascribed to the enhanced membrane monolayer protrusion as well as exert a shearing force to rupture the membrane.[6] However, the fundamental mechanism of how a vesicle responds to the active RNP remains poorly understood.

From the experimental viewpoints, the active rotation of NPs can be controlled by the underlying dynamic magnetic field. For example, the rotational movement of superparamagnetic iron oxide nanoparticles induced by dynamic magnetic field can cause membrane permeabilization and lead to apoptosis.[7] NPs are enclosed inside intracellular endosome vesicles, which can be deformed to probe the intracellular membrane, or turn into intracellular heater when subjected to magnetic field.[8, 9] Another promising application for RNPs is drug delivery. RNPs are widely used as carriers to translocate drug molecules and other useful materials into cell interiors.[10-16] The targeted RNPs have been described to control the delivery and release of anticancer drugs with advanced controllability.[17, 18] RNPs in a proper magnetic field can give rise to a local effect to

encourage drug release, for example, by way of the hyperthermia effect.[19] However the efficiency of drug loading and unloading remains challenging for RNPs. By unraveling the rudimentary behavior of a single cell interacting with a single RNP, it will offer insight into the development of drug delivery research. In this paper, we propose a simple magnetic field geometry to create a RNP channel on a single vesicle with a hollow hybrid RNP-filled channel. There has been much interest in developing synthetic analogues of biological membrane channels with high efficiency and remarkable selectivity for transporting ions and molecules.[20, 21] By using dissipative dynamics simulation, we investigate the interaction between RNPs and a vesicle under different rotational frequencies as well as the effect of RNP size and coating patterns. We also demonstrate a possible pathway of formation of the RNP-based channel for drug delivery which is executed via a diffusion process through the channel. The main advantages of RNP channels are that they (i) can be visualized, (ii) guide the drug through the channel by diffusion, and (iii) do not need a trigger for drug release. Analysis of the mechanism underlying the interaction between RNPs and a single vesicle provides insight into the molecular dynamics of cellular features. Our simulation results establish RNPs as a promising prototype of synthetic membrane channel with inherent robustness geared towards biological challenges and exceptional biocompatibility for drug delivery.

## Computational Model and Methodology

Simulations are based on dissipative particle dynamics (DPD), a mesoscopic coarse-grained simulation method for soft matter and biomembrane systems.[22, 23] In a typical DPD model, a small group of atoms is treated as a single bead located at the center of mass of the group. Beads $i$ and $j$ interact with each other via a pairwise force consisting of a conservative force $F_{ij}^{C}$ (representing excluded volume effect), a dissipative force $F_{ij}^{D}$ (representing viscous drag between

moving beads), and a random force $F_{ij}^R$ (representing stochastic impulse). Both $F_{ij}^D$ and $F_{ij}^R$ act together as a thermostat for the beads. Similar to molecular dynamics simulation, time evolution is also governed by the Newton's equation of motion. The total force on bead $i$ can be expressed as

$$F_i = \sum_{i \neq j}\left(F_{ij}^C + F_{ij}^D + F_{ij}^R\right) = \sum_{i \neq j}\left(a_{ij}\omega\left(r_{ij}\right)\hat{r}_{ij} - \gamma\omega^2\left(r_{ij}\right)\left(\hat{r}_{ij} \cdot v_{ij}\right)\hat{r}_{ij} + \sigma\omega\left(r_{ij}\right)\zeta_{ij}\Delta t^{-1/2}\hat{r}_{ij}\right) \quad (1)$$

where $a_{ij}$ is the maximum repulsive force, $r_{ij}$ the distance, $\hat{r}_{ij}$ the unit vector, and $v_{ij}$ the relative velocity between beads $i$ and $j$; $\zeta_{ij}$ denotes a random number with zero mean and unit variance, and

$$\omega\left(r_{ij}\right) = \begin{cases} 1 - \frac{r_{ij}}{r_c}, & r_{ij} < r_c \\ 0, & r_{ij} > r_c \end{cases} \quad (2)$$

is a normalized distribution function, with $r_c$ being the cutoff radius; $\gamma$ and $\sigma$ are parameters related to each other as $\sigma^2 = 2\gamma k_B T$, $k_B T$ being the unit of energy. The standard values $\sigma = 3.0$ and $\gamma = 4.5$ are used in our study.[2] The mass, length and time scales are all normalized in the DPD simulations, with the unit of length taken to be the cutoff radius $r_c$, the unit of mass to be that of the solvent beads, and the unit of energy to be $k_B T$. All other quantities are expressed in terms of these basic units. The reduced DPD unit can be converted to SI unit by examining the membrane thickness and the lipid diffusion coefficient. The simulated value of bilayer thickness is $5r_c$ and the effective time scale of the simulation can be determined from the simulated lateral diffusion constants of the lipid bilayer.[24] The DPC bilayer thickness is about 4 nm with a diffusion coefficient around 5 $\mu m^2 s^{-1}$.[25] By comparison with typical experimental values, it can be shown that one DPD length unit corresponds to approximately 0.8 nm in physical units and

the time unit to $\tau = 24.32$ ps. The force unit is $k_B T/r_c = 5.175pN$. The time step is taken as $\Delta t = 0.01\tau$. All simulations are performed using LAMMPS.[26]

The dimensions of the simulation box are $42r_c \times 42r_c \times 50r_c$. The system contains a total of 271,215 particles, 241,214 water beads, and 29,445 lipid beads with a particle density of approximately 3.[27] The solvent beads are not shown for clarity in the following figures. The simulation system is comprised of the vesicle consisting of 2,265 lipid molecules and a rigid cylindrical RNP (556 hydrophobic beads) coated with a selected pattern of ligand and solvent particles. The lipid molecule is represented by the coarse-grained model proposed by Groot and Rabone[22] as shown in Figure 1, containing 1 lipid hydrophilic head bead and 4 lipid hydrophobic tail beads. The hydrophilic bead and hydrophobic bead are shown as green and blue, respectively. The repulsive interaction parameters for the same types of beads within the RNP, ligand, and membrane are $a_{ij} = 25$, and those for two beads with different types are set as $a_{ij} = 100$. Within a lipid molecule and ligand, an elastic harmonic force,

$$F_{ij}^{S} = k_s(1 - \frac{r_{ij}}{r_s})\,\hat{r}_{ij} \tag{3}$$

is used to connect two consecutive beads, where $k_s$ and $r_s$ are the spring constant and equilibrium bond length respectively. Here we use $k_s = 100.0$, $r_s = 0.7r_c$ for lipid molecule [28] and $k_s = 200.0$, $r_s = 0.25r_c$ for ligand.[2] The ligands are also anchored to the RNP surface by a spring force $k_s = 200.0$, $r_s = 0.25r_c$ to prevent the rearrangement or detachment of coating ligands during the simulation. The bending resistance of the lipid and ligand chain is represented as an additional force due to a harmonic constraint on two consecutive bonds

$$F^{\theta} = -\nabla V_{bend} = -\nabla[k_\theta(\theta - \theta_0)^2] \tag{4}$$

where $k_\theta$ , $\theta$ and $\theta_0$ are the bending constant, inclination angle and equilibrium angle, respectively. For three consecutive lipid tail beads or three consecutive lipid head beads in a lipid molecule, we take $k_1 = 6$ and $\theta = 180^\circ$; for the last head-bead and the top two tail-beads $k_2 = 3$ and $\theta = 120^\circ$; for the bottom two consecutive head beads and the first bead in each tail $k_3 = 4.5$ and $\theta = 120^\circ$.[2] For three consecutive ligand beads, we take $k_\theta = 5$ and $\theta = 180^\circ$.

## Results and Discussions

### Effect of rotational frequencies

It has been shown that bacteria cells can move forward by rotating long thin helical filaments counterclockwise.[29, 30] Artificial bacterial flagella, ones consisting of helical tails resembling natural flagella, show a linear relationship between the frequencies of their rotation and the translational velocity.[31] Different from a filament-based motor, the motor-like RNP can tremendously affect its local biological environment, thereby exerting undeniable influence on its penetration capability into the biological tissues. To demonstrate the effect of RNP on the surrounding environment, we place the RNP on the planar membrane and characterize the membrane disturbance by calculating the local membrane curvature based on the method developed by Yue et al..[32] First of all, the RNP is put $5r_c$ away from the $40r_c \times 40r_c$ membrane surface. The RNP rotates along the vertical axis. The membrane is divided into $2r_c \times 2r_c$ vertical square prisms unit, and lipids within each unit determine the center of mass of the unit. The geometric surface representing the membrane via least-squares fitting is described in the form of quantic polynomial, $z(x, y) = \sum_{i+j\leq 5} a_{ij} x^i y^j$ , where $a_{ij}$ are fitted parameters. And the curvature $k_x$ and $k_y$ at point $(x, y)$ can be evaluated via

$$k_x = \frac{d^2z}{dx^2} \Big/ \left[1 + \left(\frac{dz}{dx}\right)^2\right]^{3/2}, \quad k_y = \frac{d^2z}{dx^2} \Big/ \left[1 + \left(\frac{dz}{dy}\right)^2\right]^{3/2} \tag{5}$$

It can be noticed, from Figure 2, that the membrane curvature keeps constant as the RNP rotates along the vertical axis. That means the vertical rotational direction of the RNP barely causes any disturbance in the membrane. However when it changes from the vertical rotational axis to the horizontal rotational axis of the RNP, RNP causes a large deformation of the planar membrane and leads to a dramatic change in the membrane curvature. In the following simulation, the rotational axis is chosen to be the longitudinal axis of the nanoparticle for the reason that it could enhance the vesicle membrane protrusion as well as exert minimal shearing force to avoid the rupture of vesicle.[6] With respect to the controllability of the rotational axis of the RNP, it has been demonstrated that in experiment the magnetic nanotube could be assembled and positioned in a controlled manner [33-35] and rotate with controlled angle, speed by magnetic field.[36, 37]

For our simulations, initially the RNP (diameter=$4r_c$, length=$10r_c$) is placed $5r_c$ away from the vesicle surface and restrained to its center-of-mass and set as default simulation model unless otherwise stated. Now the resulting NP rotation, not attached to the vesicle but rather situated around the vesicle, causes synchronized translation of water beads to match the winding geometrical movement around the RNP. Therefore the water particle can induce a locomotive force on the vesicle along the rotational axis of the RNP to drive it towards the RNP rather than inducing random contributions on the vesicle with a zero net effect. The translocation path of the vesicle is along the rotational axis of the RNP. Once the RNP starts to contact with the vesicle, the vesicle quickly internalize the RNP due to the identical hydrophobicity of the RNP and the vesicle inner layer. Here the driving force acting on the vesicle comes from the local swirling flow towards to the RNP induced by the pressure difference along the axis of the RNP. The flow

induced by the viscous drag of the RNP is the key reason that the vesicle is capable to approach to the RNP.[38]

Intuitively, the rotational frequency of RNP is critical for creating the locomotive force. It has been demonstrated that the water flux generated by a rotating carbon nanotube has approximately logarithmic dependence on the angular velocity of rotation.[39] By fixing the RNP and vesicle size, an active rotation is applied to an uncoated RNP under different rotational frequencies, creating the locomotive force to drive the vesicle slowly approach the hydrophobic RNP. The translocation path of the vesicle is perpendicular to the vertical rotation axis of NP. As shown in Figure 3, the vertical axis indicates the translocation time needed from the initial state to the state where the RNP is internalized in the vesicle. As the NP is encapsulated into the vesicle, the encapsulation degree (ED) is defined by taking the ratio of surface area covered by lipids to the whole NP surface area. When the encapsulation degree reaches the critical value 95% as shown in Figure 3 and keeps increasing or constant after the critical time step, we consider the NP is totally internalized by the vesicle. It is clearly shown that the translocation time is proportional to the rotational frequencies, with high rotational frequencies shortening the translocation time. By data fitting, the translocation time is demonstrated to be logarithmic dependent on the rotational frequencies with the estimated relationship $-558.9ln(x) + 2{,}366$. At high rotational frequencies, the increment of translocation time is much smaller than that at low rotational frequencies. At low rotational frequencies, the disturbance by RNP is neutralized by the dynamics of the water particles. However, without RNP, the vesicle barely changes its position. For the fundamental estimation of the driving force, the rotational torque generated by the RNP can be calculated from the rotational speed of the RNP. The RNP is simplified as a rotating cylinder. Under this condition, the rotational torque ($T$) is obtained by the equations

$T = \gamma\omega,\ \gamma = \frac{\frac{1}{3}\pi\eta L^3}{\ln\left(\frac{L}{2r}\right)-0.66}$, where $\gamma$ is the rotational drag coefficient, $\omega$ is the rotational speed, $\eta$ is the viscosity of the environmental solution, $L$ is the length of the cylinder, and $r$ is the radius of the cylinder.[40] Here we take $\eta = 0.001\text{Pa} \bullet \text{s}$ (pure water), $L = 10r_c$ and $r = 2.0r_c$. As a result, the rotational torque is calculated to be in the range of 0.54 nN•m to 0.0056 nN•m. It is shown that the rotational torque of the RNP could be controlled on the order of ~$10^{-1}$ to ~$10^{-3}$ nN•m. The driving force of the RNP can be controlled by varying the rotational frequencies(for detail please see the following section). Here we propose a novel method to accelerate the vesicle endocytosis of NP by rotation via controllable external magnatic field. Experimentally, the RNP channel can be embedded into the lipid membrane acting like a bological ionic channel[20] which will provide useful guidelines in designing RNP based nanodevices.

**Effect of nanoparticle shape**

The cellular internalization for NPs is dependent on their properties, like size, shape anisotropy, hydrophobicity, surface charge, and ligand arrangement.[41, 42] For example, nanotubes with small radii tends to pierce directly through the cell membrane while larger ones tend to enter the cell via wrapping mechanisms.[43] The optimal NP size for endocytosis is on the order of 25-50nm while exceedingly large or small NPs would yield an inefficient uptake.[44, 45]. The shape and size of nanoparticle have tremendous impacts on the translocation time of NPs into the vesicle. Here, in order to investigate the effect of nanoparticle shape on its internalization process into a vesicle, the rotational frequency of the RNP is fixed to be $1/(6\tau)$. By fixing the contact area with a constant diameter $4.0r_c$ between the RNP and vesicle membrane, we elongate the RNP to demonstrate the effect of the shape of RNP on its interaction with the vesicle. As shown in Figure 4, when the geometric ratio is equal to 1, the diameters of sphere RNP being equal to the bilayer

thickness of vesicle, the RNP takes the least time to be endocytosed by the vesicle. The spherical RNP finally is stuck into the middle of the bilayer of the vesicle. Interestingly, the translocation time increases quickly when the length of the RNP is raised from 1.5 to 2.1 times of its diameter. This can be explained by the size effect observed in the experiment that the large size of NP take longer time enter inside the bilayer.[44] When the aspect ratio increases to the value close to 3, RNP cannot be wrapped due to the continuous rotation of NP since there exists an energy barrier in the hydrophobic middle of the bilayer for the hydrophobic RNP[2]. This barrier creates a strong interaction between hydrophobic RNP and the hydrophobic portion of the bilayer, therefore prohibiting the further penetration of the RNP into the vesicle. Energetically, as shown in Figure 7, for all sizes of RNP, the free energy based on the method presented by Yue et al [46] decreases as hydrophobic RNP enters into the vesicles, indicating that RNP has a favorable position inside the bilayer membrane. For the large length/diameter ratio of RNP, it's easier to be trapped inside the vesicle membrane and be difficult to get out. The dependence of translocation on the RNP size is in agreement with the NP internalized by vesicles in other researcher's work.[47] From the analysis of the geometric ratio of the RNP, we have demonstrated that the length of the RNP plays an important role on the translocation time for the RNP entering inside the vesicle and provides a useful guideline to optimize the design of RNP size for its application on nanodevices.

The simulation results from Figure 3 and Figure 4 have suggested that the driving force $F$ on the vesicle may primarily depend on the following parameters: the cylindrical nanoparticle height $H$ and diameter $D$ (or the aspect ratio $H/D$), intrinsic solution properties like water viscosity $\upsilon$, angular velocity $\omega$ of the rotating nanoparticle. Since all of the simulations are performed in water and the temperature is kept unchanged, the viscosity of the water is considered as a constant. Then the independent parameters left are the aspect ratio of the nanoparticle and its

rotational angular velocity. To study the effects of these parameters on the driving force of the vesicle, in what follows we present the way the driving force on the vesicle is estimated. From the simulation snapshots of the penetration process of the nanoparticle into the vesicle as shown in Figure 3, we can notice that the vesicle under the driving force moves straightly along the vertical axis of the nanoparticle. Therefore we can assume that the motion of the vesicle is simplified to a rectilinear motion with a uniform acceleration. For a rectilinear motion with uniform acceleration, the relationship among displacement from the initial position ($S$), initial velocity ($V_0$), time ($t$), acceleration ($a$) can be expressed as $S = \frac{1}{2}at^2 + V_0t$. The displacement of the vesicle in our model can be simplified as $S = \frac{1}{2}at^2$ since the initial velocity of the vesicle is zero. By tracking the displacement of the vesicle, we can estimate the acceleration of the vesicle and further estimate the driving force through $F = m_{vesicle}a$. To begin with the effect of the angular velocity of the vesicle $\omega$, we can have the acceleration $a$ of the vesicle under RNP with different rotational frequencies as shown in Figure 5. It can be implied that the driving force on the vesicle is linearly proportional with the angular velocities where $F = k\omega$, $k$ is the slope of the fitting curve with the value of 0.03605. Similarly, we can also obtain the relationship between the driving force $F$ on the vesicle and the nanoparticle's aspect ratio $H/D$ as shown in Figure 6. By curve fitting, we can imply that the driving force has a quadratic relationship with the nanoparticle's aspect ratio $H/D$ where $F = k_1\left(\frac{H}{D}\right)^2 + k_2\left(\frac{H}{D}\right) + k_3$ with $k_1 = 0.08592$, $k_1 = -0.2118$, and $k_3 = 0.2119$.

It is interesting to further propose a scaling law from the dimensional analysis to link the driving force with the parameters such as rotational angular velocity and the nanoparticle's aspect ratio. The dimensional analysis is used to identify a complete set of independent quantities that

determine the driving force $F$ on the vesicle. Here we assume the primary factors are the viscosity of the water $\upsilon$, the height of the cylindrical nanoparticle $H$, the diameter of the cylindrical nanoparticle $D$, and the rotational angular velocity of the RNP $\omega$ .In the type of system of units, the dimensions of the quantities are: $[F] = F, [\omega] = T^{-1}, [\upsilon] = FL^{-2}T, [D] = L, [H] = L$. We choose $F$ and $D$ as dependent variables and non-dimensionalize the remaining independent variable as $\Pi_1 = \frac{F}{\omega \upsilon D^2}$ , $\Pi_2 = \frac{H}{D}$. Using Buckingham's π-theorem, we have the following relationship expresses the driving force in terms of a complete set of variables $\frac{F}{\omega \upsilon D^2} = \emptyset\left(\frac{H}{D}\right)$ From the simulation data as shown in Figures 5 and 6, we can have the relationship between $\Pi_1$ and $\Pi_2$ and the driving force acting on the vesicle can be theoretically estimated as

$$F = \omega \upsilon D^2 \left(k_1 \left(\frac{H}{D}\right)^2 + k_2 \left(\frac{H}{D}\right) + k_3\right) = \omega \upsilon (k_1 H^2 + k_2 DH + k_3 D^2) \qquad (6)$$

with $k_1 = 0.01026$, $k_1 = -0.02528$, and $k_3 = 0.0253$. It implies that the driving force is linear with the rotational angular velocity of the RNP as verified in Figure 5 and is a parabolic function with the nanoparticle's aspect ratio as evidenced in Figure 6.

**Effect of coated patterns**

Due to the extremely small size, high surface energy, and high surface area of the RNP, the interaction between cells and RNPs can be heavily influenced by intelligent surface structure designs.[48-50] Tissue and cell-specific drug targeting by RNPs can be achieved by employing specific coatings to the RNPs or carrier-drug conjugates which contain a ligand recognized by a receptor on the target cell.[51, 52] RNPs modified with synthetic ligands can bind to both Gram-positive and Gram-negative bacteria to clear them and their related endotoxins from the bloodstream.[53] It turns out that the surface modification is a very important controller to the

interaction between RNPs and cells. Based on the arrangement of the ligands on the RNP's surface, here we test four coating patterns as shown in Figure 8: left-half coated, upward-half coated, downward-half coated, fully coated. By rotating the NPs, the attached ligand will also follow its rotation. As expected, the pure hydrophobic RNP can piece through the vesicle membrane easily while the portion of the RNP coated with hydrophilic ligand cannot get through the vesicle membrane when the driving force is insufficient to overcome the repulsive force due to hydrophobicity of the middle layer of the membrane. For the pure RNP, when the rotation creates the upward driving force for the vesicle, the vesicle moves toward the RNP and the RNP starts to pierce into the vesicle and is locked inside the middle of the vesicle membrane as we discussed in previous section. However, the driving force cannot overcome the size-dependent penetration force (~60 $k_BT/r_c$ [54]) for the RNP passing through the vesicle membrane. For the downward-half coated and full coated, the hydrophilic ligand prohibits further movement of the vesicle due to the hydrophilic interaction between the ligand and hydrophilic vesicle surface as well as the interaction between the ligand and solvent. For the upward-half coated, obviously, the uncoated portion of the RNP can penetrate the vesicle membrane, but further movement is inhibited by the coated hydrophilic ligand. Through the surface coating study, we can demonstrate that vesicle movement and cellular uptake capability triggered by the RNP can be controlled by sophisticated surface design of the RNP.[50]

Figure 9 quantitatively dictates the interaction energy profile between the uncoated or patterned RNP with the vesicle as simulation time goes on. For (a) uncoated RNP and (c) upward coating, the pressure field round the vesicle created by the NP rotation is lower than that created by the hybrid RNP rotation for patterns (b) and (d). For (a) and (c), the interaction between the uncoated RNP and vesicle experiences a transitional stage in agreement with the slowly moving vesicle,

however, it remains constant after the RNP is locked in the middle layer of the membrane. With a strong driving force created by the ensemble rotation of NP and ligands, for coatings (b) and (d) the vesicle takes less time to approach the RNP than those for coatings (a) and (c). However, the hybrid RNP is incapable of penetrating into the vesicle membrane after reaching the closest tip of the RNP for coatings (b), (d) and (e). From the analysis of the energy profile, it offers a better understanding that the coating ligand plays a tunable role in creating an energy barrier and further regulating the movement path of vesicles.

**Drug delivery channel**

NPs are known to have high drug-loading capacity, high water solubility, and an appropriate size for long circulation in the blood.[55-57] The drug unloading process is typically limited to stimuli such as pH [58, 59], temperature [60], light [61] etc. However the efficiency of drug loading and unloading remains challenging for drug delivery devices. From the fundamental behavior of a single vesicle interacting with a single RNP, here we would like to demonstrate a novel drug delivery process by integrating a nanochannel into a vesicle through the NP-rotating mechanism. In this model, all representative drug molecules are assigned to be a single bead, and are uniformly distributed and ideally mixed in the solvent by allowing the solution to run for 2000τ under NVE conditions. The interaction between drug beads and water beads is defined to be $a_{\text{drug-water}} = 25$ (close to $a_{\text{water-water}} = 25$) to avoid forming drug clustering or precipitation before transporting into the vesicle. The interaction between drug beads and lipid beads is defined to be $a_{\text{drug-hydrophobic beads}} = 100$, $a_{\text{drug-hydrophilic beads}} = 25$. In order to investigate the effect of the drug concentration outside the vesicle, it has been varied with a set of 10%, 20%, 40%, 60%, and 80% for each trial. The RNP with $12r_c$ (three times the membrane

thickness $4r_c$) is coated over one third of its surface area by hydrophilic ligands on the upward tip, similar to the pattern in Figure 8(c). The downward tip is designed as a spherical cap which introduces minimum disruption on the vesicle membrane during the rotation [62] with a lipid-size pore. The size of lipid-size pore is chosen as the maximal value wherein none of the membrane lipid can pass into the RNP. The rotational frequency of the RNP is set to be 1/(6τ). Figure 10 depicts the dynamic evolution of the drug delivery process. The water beads are not shown for clarity. Following the rotation of the NP, the vesicle closely approaches the RNP and the hydrophobic RNP is immersed inside the membrane until the part of RNP with the ligand coating prohibits further penetration. After stabilization, the constraint for the RNP is released and the rotation is stopped as well to minimize perturbation on the membrane. Then, through self-diffusion process, the drug beads slowly enter inside the RNP core and get into the interior of the vesicle. The diffusion process from outside of the vesicle with a high concentration of drug beads to the interior regions with a low concentration of drug beads takes long time to reach an equilibrium state where the concentrations inside and outside are similar. The number of drug beads passing through the RNP channel entering inside the vesicle is counted in Figure 11. Following the penetration of the RNP into the vesicle to form the stable channel at 1000τ, the drug outside the vesicle initiates the slow diffusion across the RNP channel to get inside the vesicle. Due to the different concentration of drug beads outside of the vesicle, the drug concentration inside the vesicle monotonically increases until the balanced state reaches. The diffusive rate is linearly proportional to the number of drug beads inside the vesicle and can be described by $r = \frac{\partial N}{\partial t}$ in the single direction along the RNP channel, where $N$ is the number of drug beads appearing inside vesicle, $t$ is the time needed for diffusion. The diffusive rate of drug differs as 0.25 bead/τ, 0.19 bead/τ, 0.12 bead/τ, 0.06 bead/τ, and 0.03 bead/τ by calculating the

slope of the curve in Figure 11 for drug concentrations of 80%, 60%, 40%, 20%, and 10% respectively. The corresponding concentration of drug inside the vesicle is 73.5%, 55.1%, 36.8%, 18.4%, and 9.1% at the final equilibrium state. Eventually the drug concentration inside and outside the vesicle is close to each other. Based on the analysis of the drug delivery process promoted by RNP, we illustrate that the hybrid RNP with a hollow core can efficiently improve the drug delivery efficiency and greatly increase the popularity of its biomedical applications.

## Concluding remarks

In summary, we have performed dissipative particle dynamics simulation to investigate how the RNP affects its local environment and triggers the movement of an adjacent vesicle toward it by controlling its shape, surface chemistry and rotational frequency. The translocation time needed for the RNP to enter the vesicle decreases with the decrease of rotational frequencies while it increases with the increase of its aspect ratio. Our simulation results also suggest that RNPs with patterned surfaces can help open channels in the vesicle membrane, and provides a novel design to enhance the drug delivery efficiency via diffusion process for drug delivery systems while maintaining the integrity of the vesicle structure. Meanwhile, there is still a plenty of room for further exploration on modifying the properties of RNPs to tune its drug selectivity. For example, cell swelling generally occurs because of the osmotic pressure created either by an ionic imbalance, or by a lack of nutrients. Under either circumstance, the cell expands to cope with the imbalance of the chemicals it needs through various channels for maintaining its metabolism. We hope our fundamental simulation findings can stimulate the research for designing novel synthetic channels by using hybrid RNPs for biomedical purposes.

## Acknowledgements

The authors acknowledge support from the University of Georgia (UGA) start-up fund. The facility support for modeling and simulations from the UGA Advanced Computing Resource Center are greatly appreciated.

## Additional information

Competing financial interests: The authors declare no competing financial interests.

## References


1. L. Zhang and X. Wang, *RSC Advances*, 2015, 5, 11776-11785.
2. Y. Li, X. Li, Z. Li and H. Gao, *Nanoscale*, 2012, 4, 3768-3775.
3. Y. Li, H. Yuan, A. von dem Bussche, M. Creighton, R. H. Hurt, A. B. Kane and H. Gao, *PNAS*, 2013, 110, 12295-12300.
4. C. Huang, Y. Zhang, H. Yuan, H. Gao and S. Zhang, *Nano Letters*, 2013, 13, 4546-4550.
5. R. Vácha, F. J. Martinez-Veracoechea and D. Frenkel, *Nano Letters*, 2011, 11, 5391-5395.
6. T. Yue, X. Zhang and F. Huang, *Soft Matter*, 2015, 11, 456-465.
7. E. Zhang, M. F. Kircher, M. Koch, L. Eliasson, S. N. Goldberg and E. Renström, *ACS Nano*, 2014, 8, 3192-3201.
8. C. Wilhelm and F. Gazeau, *J. Magn. Magn. Mater.*, 2009, 321, 671-674.
9. M. Bañobre-López, A. Teijeiro and J. Rivas, *Rep. Prac. Oncol. Radiother.*, 2013, 18, 397-400.
10. J. Klostergaard and C. E. Seeney, *Maturitas*, 2012, 73, 33-44.
11. B. Polyak and G. Friedman, *Expert Opinion on Drug Delivery*, 2009, 6, 53-70.
12. G. Ciofani, V. Raffa, Y. Obata, A. Menciassi, P. Dario and S. Takeoka, *Curr. Nanosci.*, 2008, 4, 212-218.
13. J. Dobson, *Drug Dev. Res.*, 2006, 67, 55-60.
14. R. Singh and J. W. Lillard Jr, *Exp. Mol. Pathol.*, 2009, 86, 215-223.
15. F. Gazeau, M. Levy and C. Wilhelm, *Nanomedicine*, 2008, 3, 831-844.
16. C. Sun, J. S. H. Lee and M. Zhang, *Adv. Drug Delivery Rev.*, 2008, 60, 1252-1265.
17. Z. Zhao, D. Huang, Z. Yin, X. Chi, X. Wang and J. Gao, *J. Mater. Chem.*, 2012, 22, 15717-15725.
18. V. Mody, A. Cox, S. Shah, A. Singh, W. Bevins and H. Parihar, *Appl. Nanosci.*, 2014, 4, 385-392.
19. K. Hayashi, K. Ono, H. Suzuki, M. Sawada, M. Moriya, W. Sakamoto and T. Yogo, *ACS Appl. Mater. Interfaces*, 2010, 2, 1903-1911.
20. J. Geng, K. Kim, J. Zhang, A. Escalada, R. Tunuguntla, L. R. Comolli, F. I. Allen, A. V. Shnyrova, K. R. Cho, D. Munoz, Y. M. Wang, C. P. Grigoropoulos, C. M. Ajo-Franklin, V. A. Frolov and A. Noy, *Nature*, 2014, 514, 612-615.
21. L. Franceschini, M. Soskine, A. Biesemans and G. Maglia, *Nat. Commun.*, 2013, 4, 2415.
22. R. D. Groot and K. L. Rabone, *Biophys. J.*, 2001, 81, 725-736.
23. R. D. Groot and P. B. Warren, *J. Chem. Phys.*, 1997, 107, 4423-4435.
24. X. Li, Y. Liu, L. Wang, M. Deng and H. Liang, *Phys. Chem. Chem. Phys.*, 2009, 11, 4051-4059.
25. J. C. Shillcock and R. Lipowsky, *Nat. Mater.*, 2005, 4, 225-228.
26. S. Plimpton, *J. Comput. Phys.*, 1995, 117, 1-19.
27. S. O. Nielsen, B. Ensing, V. Ortiz, P. B. Moore and M. L. Klein, *Biophys. J.*, 2005, 88, 3822-3828.
28. M. Venturoli, B. Smit and M. M. Sperotto, *Biophys. J.*, 2005, 88, 1778-1798.
29. N. C. Darnton, L. Turner, S. Rojevsky and H. C. Berg, *J. Bacteriol.*, 2007, 189, 1756-1764.
30. W. R. DiLuzio, L. Turner, M. Mayer, P. Garstecki, D. B. Weibel, H. C. Berg and G. M. Whitesides, *Nature*, 2005, 435, 1271-1274.
31. L. Zhang, J. J. Abbott, L. Dong, K. E. Peyer, B. E. Kratochvil, H. Zhang, C. Bergeles and B. J. Nelson, *Nano Letters*, 2009, 9, 3663-3667.
32. T. Yue, S. Li, X. Zhang and W. Wang, *Soft Matter*, 2010, 6, 6109-6118.
33. C. M. Hangarter and N. V. Myung, *Chem. Mater.*, 2005, 17, 1320-1324.
34. M. Fujiwara, E. Oki, M. Hamada, Y. Tanimoto, I. Mukouda and Y. Shimomura, *J. Phys. Chem. A*, 2001, 105, 4383-4386.
35. X. Jia, W. Li, X. Xu, W. Li, Q. Cai and X. Yang, *ACS Appl. Mater. Interfaces*, 2015, 7, 3170-3179.

36. K. Kim, X. Xu, J. Guo and D. L. Fan, *Nat Commun*, 2014, 5, 3632.
37. A. Ghosh and P. Fischer, *Nano Letters*, 2009, 9, 2243-2245.
38. F. M. White, *Viscous Fluid Flow*, McGraw-Hill, New York, 1991.
39. J. Feng, H. Ding, C. Ren and Y. Ma, *Nanoscale*, 2014, 6, 13606-13612.
40. J. Howard, *Mechanics of Motor Proteins and the Cytoskeleton*, Palgrave Macmillan, London, 2001.
41. E. C. Wang and A. Z. Wang, *Integr. Biol.*, 2014, 6, 9-26.
42. H. Gao, *J. Mech. Phys. Solids*, 2014, 62, 312-339.
43. X. Shi, Y. Kong and H. Gao, *Acta Mech. Sin.*, 2008, 24, 161-169.
44. S. Zhang, J. Li, G. Lykotrafitis, G. Bao and S. Suresh, *Adv. Mater.*, 2009, 21, 419-424.
45. H. Gao, W. Shi and L. B. Freund, *PNAS*, 2005, 102, 9469-9474.
46. T. Yue, X. Zhang and F. Huang, *Soft Matter*, 2014, 10, 2024-2034.
47. X. Chen, F. Tian, X. Zhang and W. Wang, *Soft Matter*, 2013, 9, 7592-7600.
48. A. Verma, O. Uzun, Y. Hu, Y. Hu, H.-S. Han, N. Watson, S. Chen, D. J. Irvine and F. Stellacci, *Nat. Mater.*, 2008, 7, 588-595.
49. A. E. Nel, L. Madler, D. Velegol, T. Xia, E. M. V. Hoek, P. Somasundaran, F. Klaessig, V. Castranova and M. Thompson, *Nat. Mater.*, 2009, 8, 543-557.
50. L. Zhang, M. Becton and X. Wang, *J. Phys. Chem. B*, 2015, 119, 3786-3794.
51. A. K. Gupta, C. Berry, M. Gupta and A. Curtis, *IEEE Trans. Nanobiosci.*, 2003, 2, 255-261.
52. K. E. Scarberry, E. B. Dickerson, J. F. McDonald and Z. J. Zhang, *J. Am. Chem. Soc.*, 2008, 130, 10258-10262.
53. J.-J. Lee, K. J. Jeong, M. Hashimoto, A. H. Kwon, A. Rwei, S. A. Shankarappa, J. H. Tsui and D. S. Kohane, *Nano Letters*, 2013, 14, 1-5.
54. K. Yang and Y.-Q. Ma, *Nat. Nanotechnol.*, 2010, 5, 579-583.
55. Z. Ahmad, A. Shah, M. Siddiq and H. B. Kraatz, *Rsc Advances*, 2014, 4, 17028-17038.
56. N. Nasongkla, E. Bey, J. Ren, H. Ai, C. Khemtong, J. S. Guthi, S.-F. Chin, A. D. Sherry, D. A. Boothman and J. Gao, *Nano Lett.*, 2006, 6, 2427-2430.
57. K. Miyata, R. J. Christie and K. Kataoka, *React. Funct. Polym.*, 2011, 71, 227-234.
58. H. Ding and Y. Ma, *Sci Rep*, 2013, 3, 2804.
59. K. Huh, H. Kang, Y. Lee and Y. Bae, *Macromol. Res.*, 2012, 20, 224-233.
60. A. A. Manzoor, L. H. Lindner, C. D. Landon, J. Y. Park, A. J. Simnick, M. R. Dreher, S. Das, G. Hanna, W. Park, A. Chilkoti, G. A. Koning, T. L. ten Hagen, D. Needham and M. W. Dewhirst, *Cancer research*, 2012, 72, 5566-5575.
61. S. Kumar, J.-F. Allard, D. Morris, Y. L. Dory, M. Lepage and Y. Zhao, *J. Mater. Chem.*, 2012, 22, 7252-7257.
62. X. Shi, A. von dem Bussche, R. H. Hurt, A. B. Kane and H. Gao, *Nat. Nano.*, 2011, 6, 714-719.

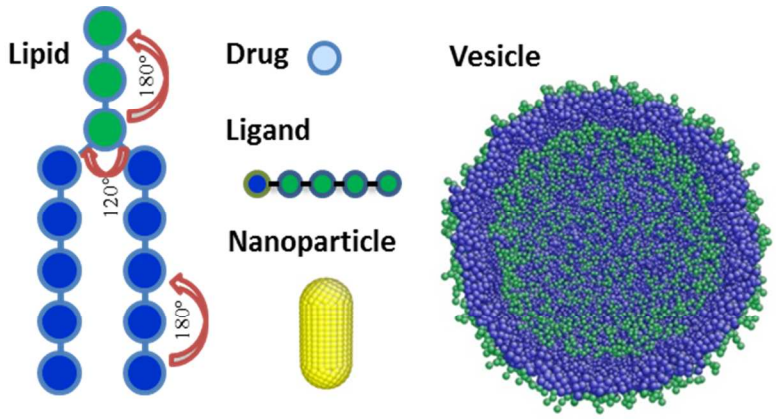


Figure 1. Schematic representation of dissipative particle dynamics model. In the following figure, unless otherwise stated, the hydrophobic bead is shown in blue while the hydrophilic is shown in green. The length of ligands is fixed as 5 (one hydrophobic bead and 4 hydrophilic beads).

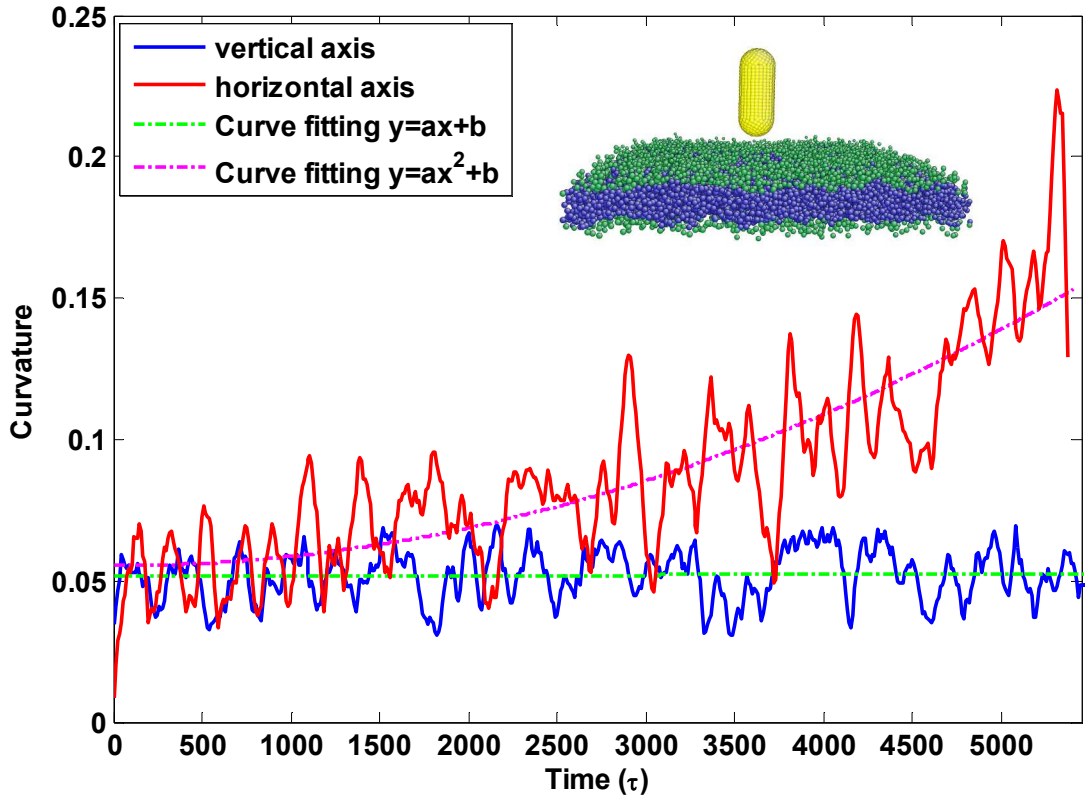


Figure 2. Evolution of the maximal curvature of the planar membrane under the rotating nanoparticle vs. the simulating time

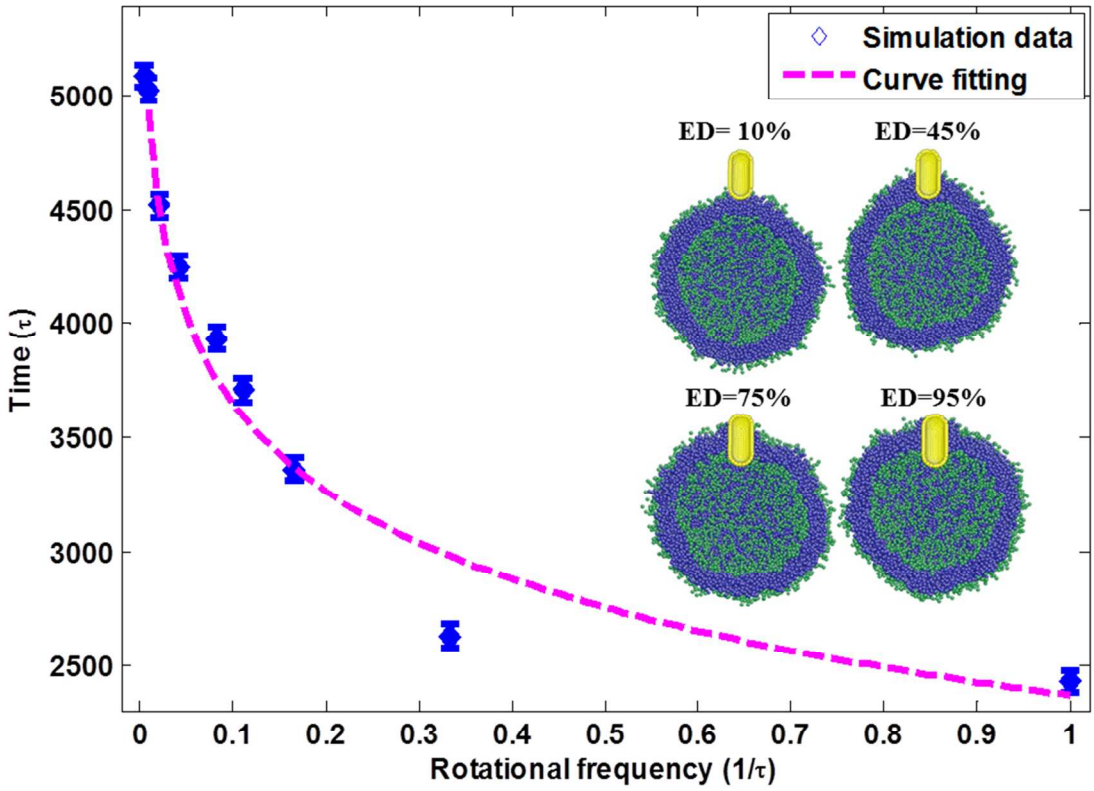


Figure 3. Contact time of RNPs and vesicle versus the rotation frequencies of the RNP

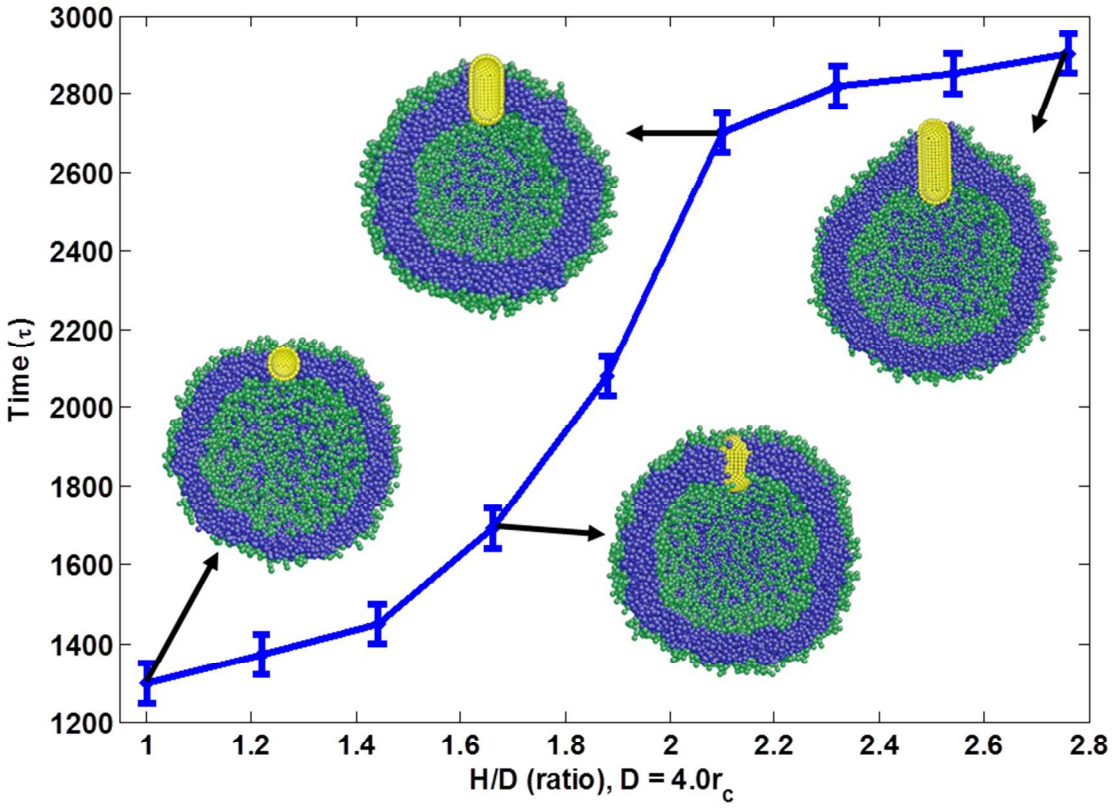


Figure 4. Time evolution of the interaction between RNPs and vesicle versus RNP shape

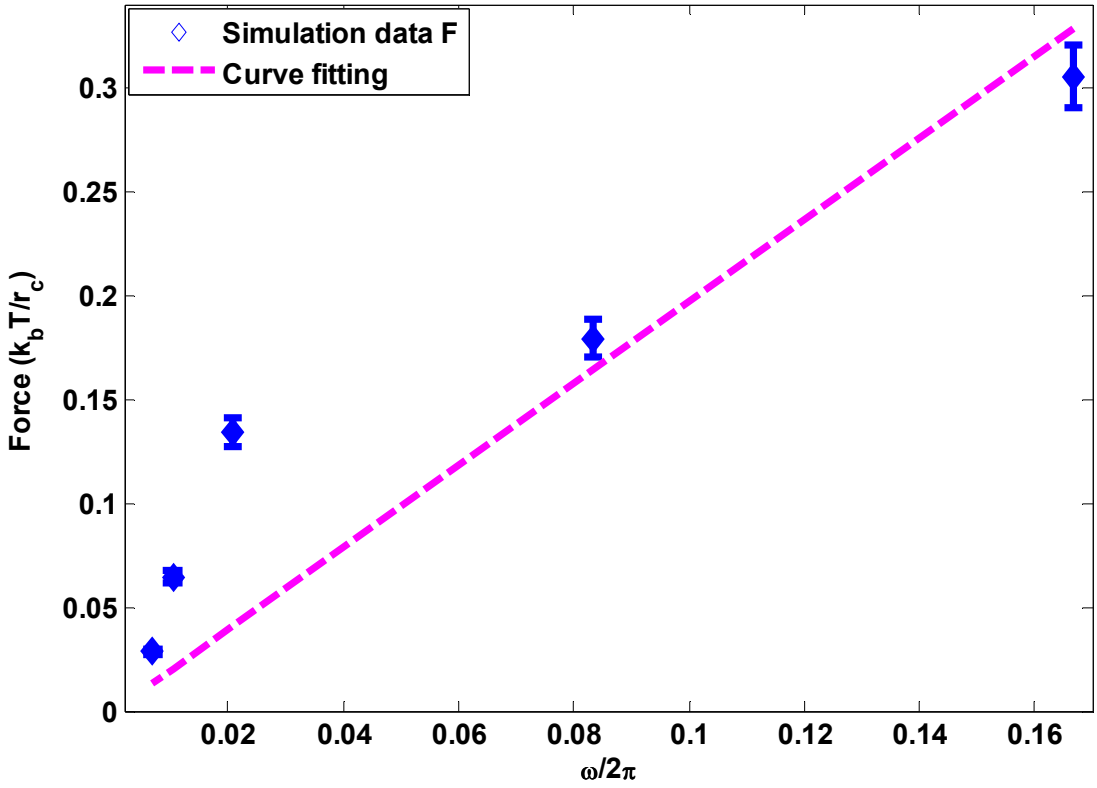


Figure 5. Relationship between the driving force on the vesicle and rotational frequencies of RNP

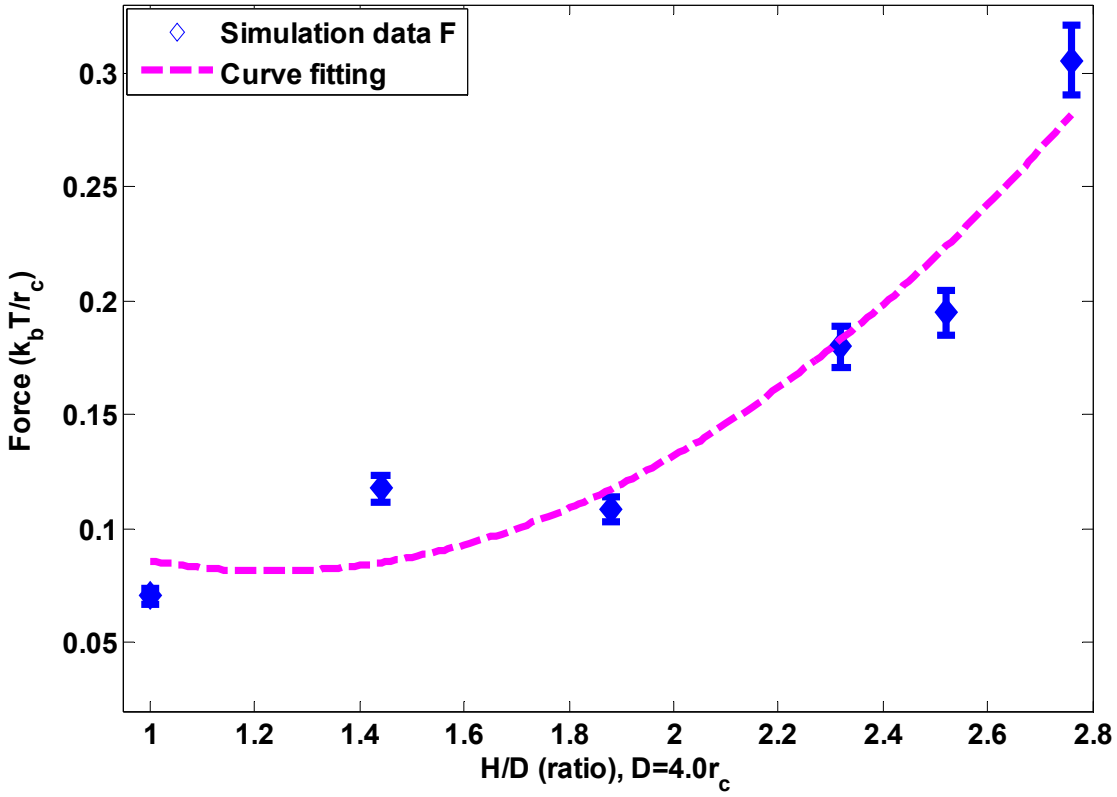


Figure 6. Relationship between the driving force on the vesicle and the nanoparticle's aspect ratio $\boldsymbol{H/D}$.

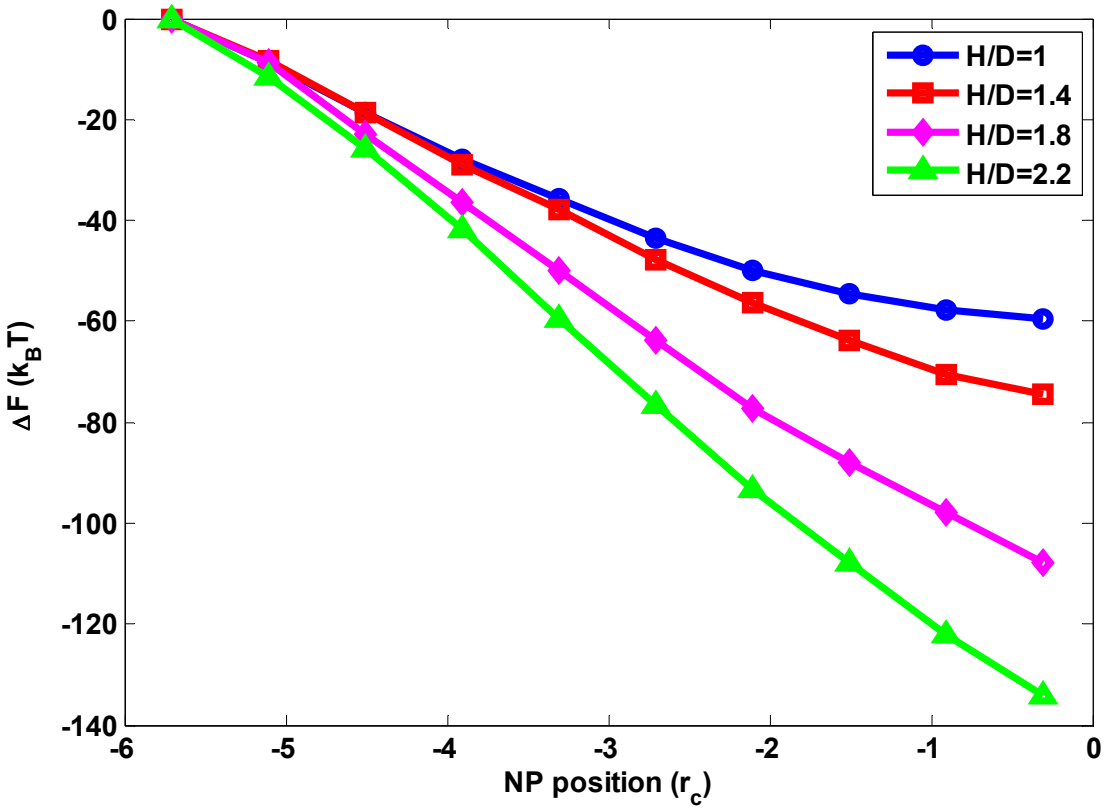


Figure 7. Free energy change for different size of RNP as a function of NP position

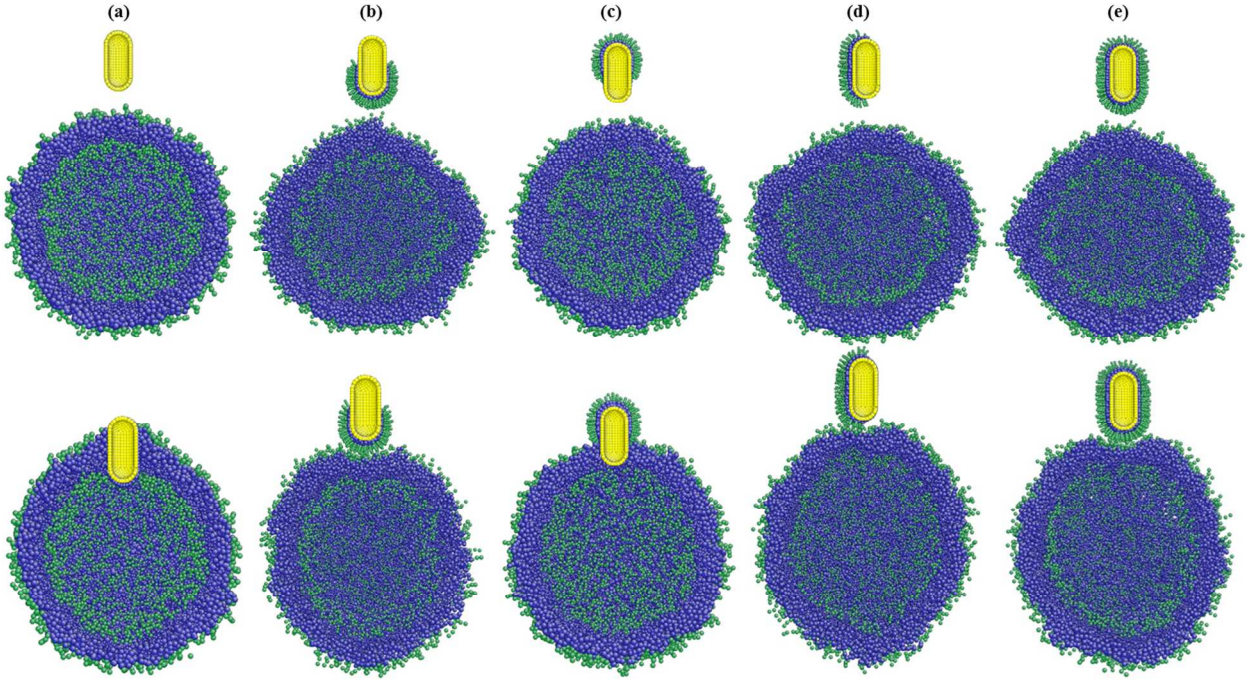


Figure 8. Dynamic process of RNPs interacting with a vesicle for five types of coating patterns. (a). No coating (b) downward-half (c)upward-half (d)left-half (e) full

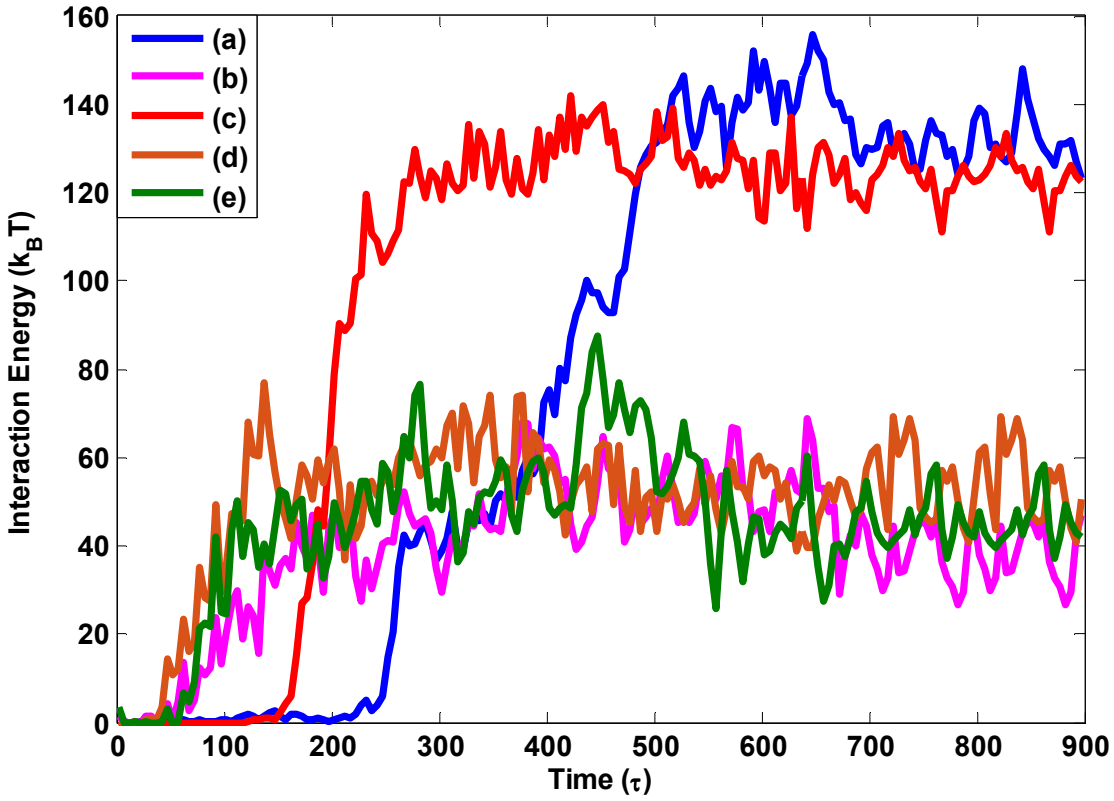


Figure 9 Energy evolution between RNP and a vesicle. (a) – (e) represents each coating pattern shown in Figure 8, respectively.

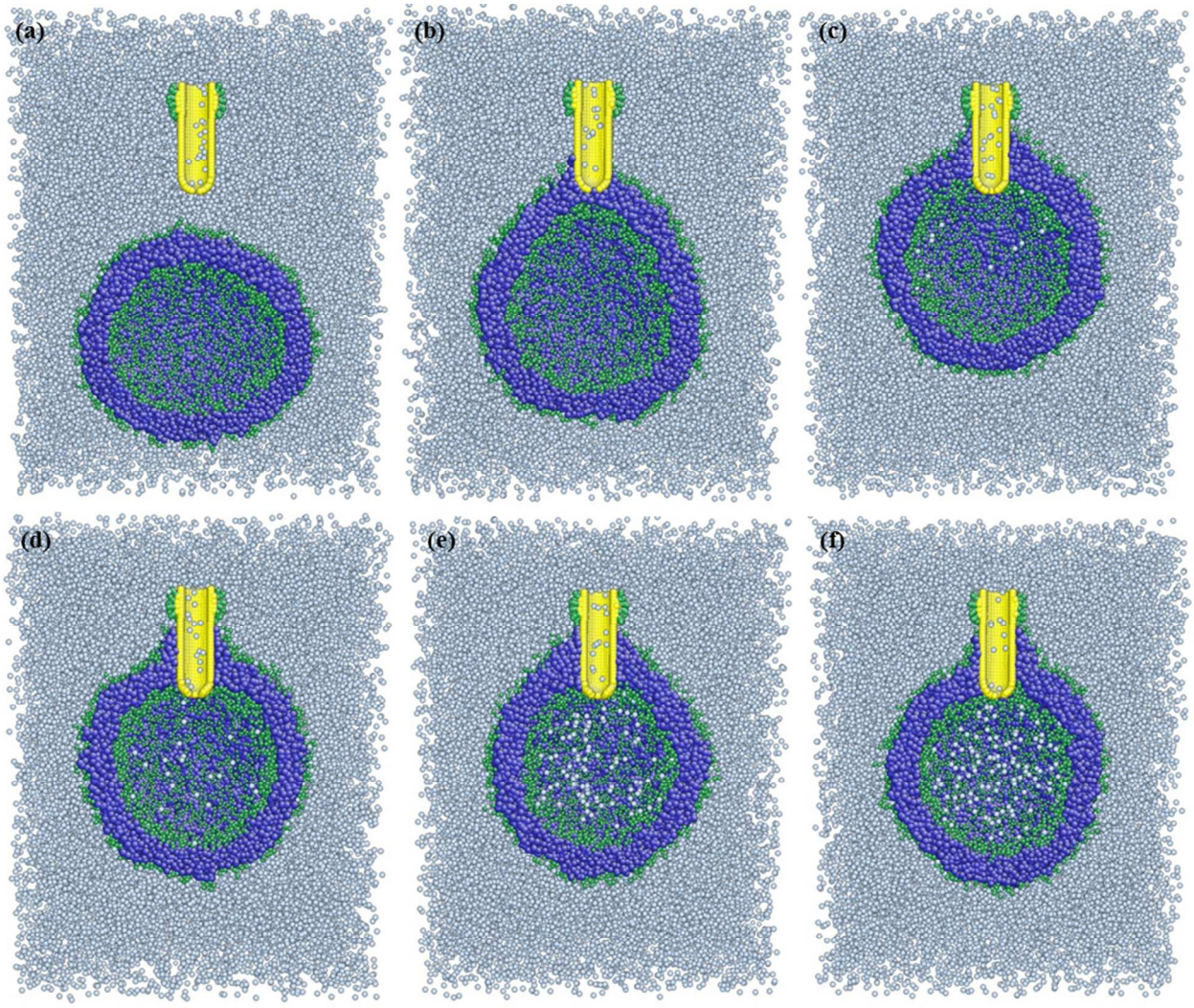


Figure 10. Dynamic process of drug delivery by using RNP's channel. (a) – (e) shows the penetration process by RNP. (d)-(f) shows the drug diffusion process through the RNP channel. The drug beads are shown in white.

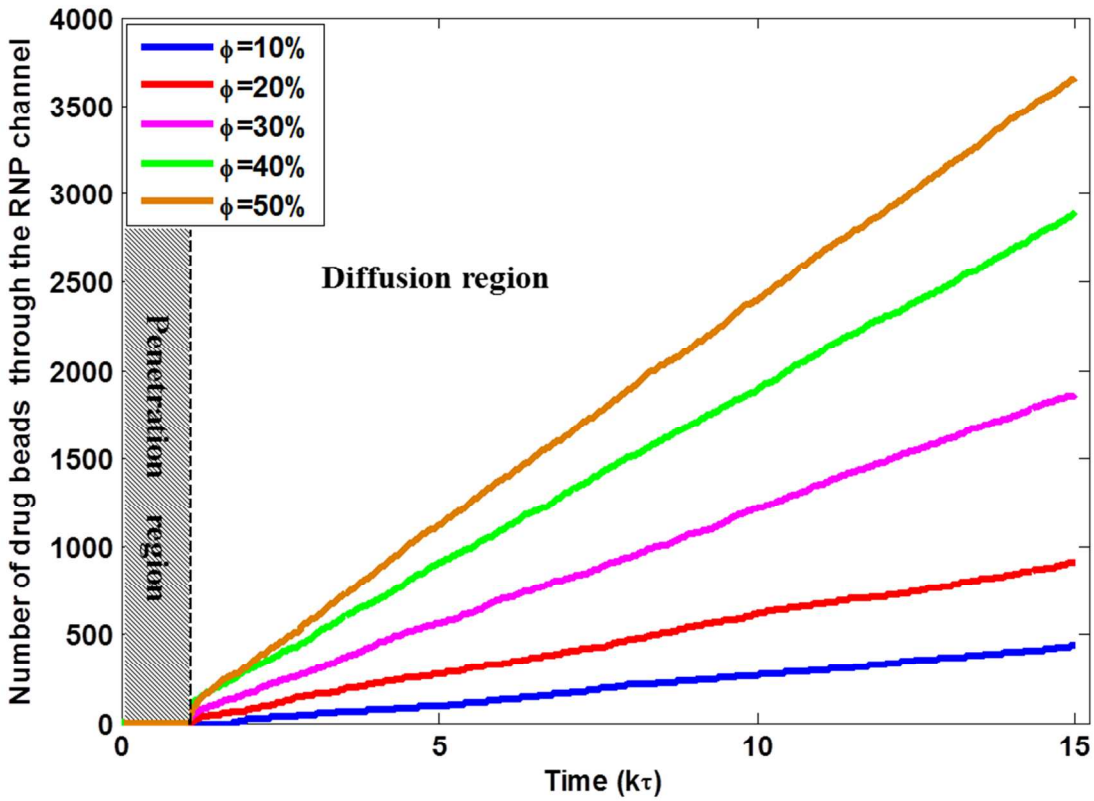


Figure 11. Evolution of drug beads numbers inside the vesicle under different drug concentrations from 10% to 80%.